Sulfur and Nitrogen Co-Doped Graphene for Metal-Free Catalytic Oxidation Reactions

Xiaoguang Duan, Kane O' Donnell, Hongqi Sun, Yuxian Wang, and Shaobin Wang**

Sulfur and nitrogen co-doped reduced graphene oxide (rGO) is synthesized by a facile method and demonstrated remarkably enhanced activities in metal-free activation of peroxymonosulfate (PMS) for catalytic oxidation of phenol. Based on first-order kinetic model, S–N co-doped rGO (SNG) presents an apparent reaction rate constant of 0.043 ± 0.002 min^{-1}, which is 86.6, 22.8, 19.7, and 4.5-fold as high as that over graphene oxide (GO), rGO, S-doped rGO (S-rGO), and N-doped rGO (N-rGO), respectively. A variety of characterization techniques and density functional theory calculations are employed to investigate the synergistic effect of sulfur and nitrogen co-doping. Co-doping of rGO at an optimal sulfur loading can effectively break the inertness of carbon systems, activate the sp^2-hybridized carbon lattice and facilitate the electron transfer from covalent graphene sheets for PMS activation. Moreover, both electron paramagnetic resonance (EPR) spectroscopy and classical quenching tests are employed to investigate the generation and evolution of reactive radicals on the SNG sample for phenol catalytic oxidation. This study presents a novel metal-free catalyst for green remediation of organic pollutants in water.

1. Introduction

Graphene, a sp^2-hybridized honeycomb lattice carbon, has emerged as a novel nanocarbon in recent years. Unique electronic, physical, and chemical properties have made it a promising candidate for versatile applications in solar cells, lithium ion batteries, biosensors, and supercapacitors.[1–5] Recent studies have demonstrated that graphene can be employed as a metal-free catalyst for various heterogeneous reactions of oxygen-reduction reaction (ORR), oxidative dehydrogenation (ODH) of alkanes, chemical synthesis, and environmental remediation, opening up a new material platform toward green and sustainable catalysis.[6–9]

Graphene can be obtained through micromechanical exfoliation, chemical vapor deposition (CVD), or reduction of chemically exfoliated graphene oxide (GO) platelets.[10] The zero band-gap of pristine graphene was suggested to greatly limit the catalytic activity and has hindered its further applications.[11] Chemical doping has demonstrated to be an excellent strategy to break the inertness of the graphene layer and to modulate the electronic and chemical properties by tailoring the electron states (charge or/and spin density) within the graphene basal plane.[12]

Substitutional doping with adventitious B, P, N, or S atoms into the carbon framework can modulate the chemical properties, create new active sites, and dramatically enhance the catalytic activity of graphene.[5,13,14] Furthermore, co-doping by two or three elements with different electronegativities can give rise to a unique electron distribution and then result in a synergistic effect.[12] Zhao et al.[15] indicated that

X. Duan, Dr. H. Sun, Y. Wang, Prof. S. Wang
Department of Chemical Engineering
Curtin University
GPO Box U1987, WA 6845, Australia
E-mail: H.sun@curtin.edu.au;
Shaobin.wang@curtin.edu.au
Dr. K. O'Donnell
Department of Imaging and Applied Physics
Curtin University
GPO Box U1987, WA 6845, Australia

DOI: 10.1002/smll.201403715

simultaneous introduction of B and N to adjacent positions of the carbon nanotube (CNT) honeycomb lattice created a neutralization effect between the electron donator (N) and acceptor (B). Zheng et al.[16] incorporated B atoms into N-doped graphene and discovered that the guest dopants were able to significantly enhance the activity of pyridinic N through a B–C–N bridge, resulting in synergistic coupling between the dopants (B and N).

Notwithstanding that nanocarbons have been intensively investigated in many catalytic processes, very few studies have been focused on graphene materials for aqueous phase catalytic reactions. In a pioneering study, we first reported that reduced graphene oxide exhibited notable catalysis in peroxymonosulfate (PMS) activation.[17] It was proposed that sp^2 carbon with abundant free-flowing electrons and unconfined π electrons at the zigzag edges can effectively react with PMS to produce reactive radicals for phenol decomposition.[18] Further physical and chemical activation approaches were applied to modify the microstructure and surface features of graphene material.[19,20] The specific surface area (SSA) was increased to a large extent and more defect sites were created for improving adsorption and catalysis. It was further found that compositional modification with nitrogen atoms doped into graphene can produce more significant enhancement for catalytically oxidative phenol degradation.[9] The doped nitrogen with a lone-pair electrons and higher electronegativity could act as the Lewis basic sites (pyridinic and pyrrolic N) to effectively activate the positively charged neighboring sp^2 carbon atoms via charge transfer (quaternary N) and disrupt the chemically inert nature of graphene network.[21]

Significant improvements in ORR via co-doping motivated us to investigate whether co-doping of other heteroatoms (B, P, S, or I) with N could bring about new properties and further promote the catalysis on nitrogen doped graphene.[22–24] Our previous study found that co-doping with trace amounts of boron (0.1 wt% B_2O_3) was able to slightly improve the catalytic activity of N-doped graphene for phenol oxidative degradation, whereas co-doping with phosphorus did not show any effect.[9] It can be also observed in Figure S1, Supporting Information that co-doping with iodine cannot further improve the activity for phenol oxidation. In this study, we employed various graphene derivatives as metal-free catalysts for PMS activation. Co-doping with sulfur greatly enhanced the catalytic efficiency of nitrogen doped graphene, suggesting that sulfur can act as a promising co-dopant to further improve the activity of chemically modified graphene toward PMS activation.

2. Results and Discussion

2.1. Characterization of Materials

The morphologies and structure of GO and S–N co-doped rGO (SNG) were obtained from SEM (scanning electron microscopy) and TEM (transition electron microscopy) images. **Figure 1**a shows that, different from the smooth surface of GO (Figure S2, Supporting Information), silk-like wrinkled flakes and several stacked layers were observed on SNG. It was reported that the wrinkled sheets were

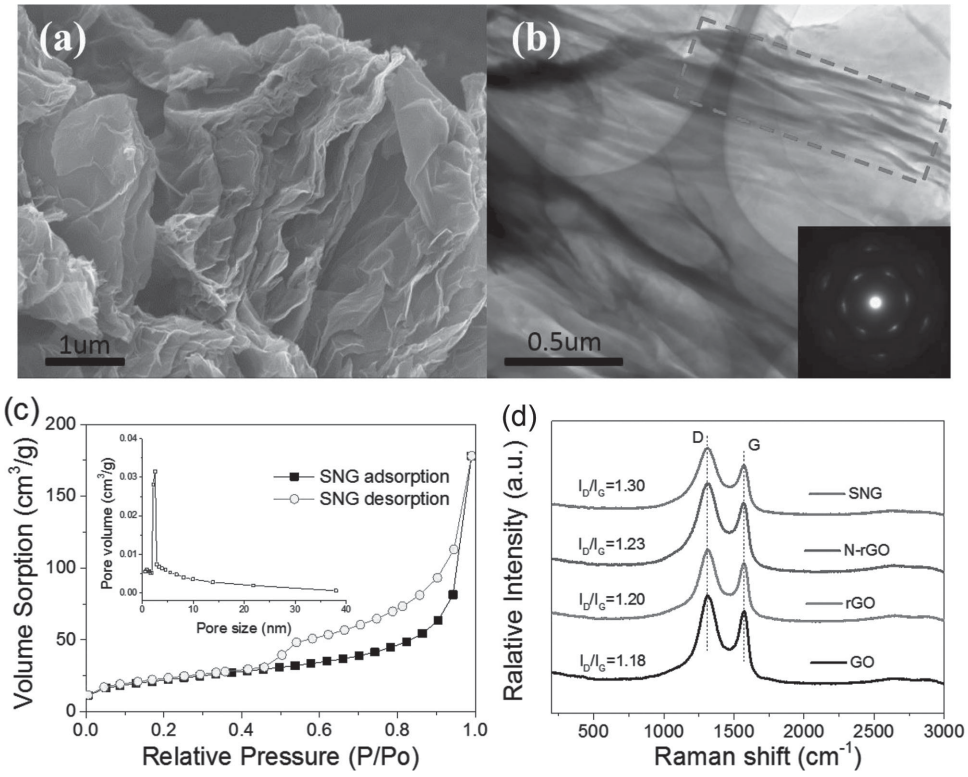

Figure 1. a) SEM image and b) TEM image of S–N co-doped graphene and SAED (inset), c) N_2 sorption and pore size distribution of SNG, and d) Raman spectra of GO, rGO, N-rGO, and SNG.

originated from the reconstruction of graphene during thermal annealing. Moreover, the defective sites produced by the heteroatom doping process would further influence the refabrication procedure, leading to more compacted and disoriented features of graphene.[25,26] TEM image in Figure 1b also revealed the stacked aggregates of SNG with wrinkled graphene sheets and the selected area electron diffraction (SAED) spot rings can be assigned to the hexagonal structure of honeycomb carbon lattice and graphite planes.[17,27] The interlayer spacing reduced from 0.83 nm (GO) to 0.34 nm (SNG) was shown in Figure S3, Supporting Information. During the doping process, more oxygen groups were removed and a better reducibility was achieved, leading to stronger π–π stacking between sp^2-hybridized graphene basal planes. The changes in chemical compositions and surface functional groups were also revealed by the characterizations such as XRD (X-ray diffraction) in Figure S3, Supporting Information, and X-ray photoelectron spectroscopy (XPS) studies. Moreover, the enhanced catalytic performances were attributed to these modifications.[28]

Figure 1c displays that the pore structure of SNG mainly had a mesopore distribution. Figure S4, Supporting Information, shows that the SSAs of GO, reduced graphene oxide (rGO), N-doped rGO (N-rGO), and SNG were 29.9, 255.4, 81.5, and 69.1 $m^2\ g^{-1}$, respectively. The SSA of rGO increased significantly after thermal annealing owing to the expansion and exfoliation of graphene layers. Heat treatment can contribute to expanding graphene layers, removing surface oxides and reducing the interaction between layers due to the removal of water and functional groups at the surface and edges of graphene. However, the SSA of rGO decreased to some extents after doping with nitrogen and sulfur atoms, which was in consistent with the distortion and multilayered structure observed in the SEM and TEM imaging. The decreased SSA of doped samples might be due to the lower exfoliation degree induced by the reduction/annealing processes with the presence of nitrogen and sulfur precursors. The intercalation of dopants resulted in the highly misorientated and crinkled structure to graphene planes, also prevented the formation of few layered structure.[29]

Raman spectroscopy is a very powerful tool to evaluate the structure of nanocarbons and the quantity of exposed edges.[30,31] Two peaks at 1310 and 1570 cm^{-1} observed in Figure 1d are corresponding to the D band and G band, respectively, and no obvious shifts were found. The D band usually results from the defects and distortion of carbon layers while the G band is closely related to the crystalline and graphitic structure.[29,32] Therefore, the intensity ratio of D to G (I_D/I_G) can clearly indicate the defect degrees of carbon materials. Generally, introducing heteroatoms into the graphene network would create more defective sites and then increase the I_D/I_G ratio.[33] Specifically, the I_D/I_G value of rGO (1.20) is slightly higher than the GO (1.18), which was possibly attributed to the decays in graphene sheets and creation of more active edges during the thermal reduction process.[20] Compared with rGO, I_D/I_G ratios were enhanced after incorporating with N atoms (N-rGO, 1.23) and co-doping with N and S atoms (SNG, 1.30) into the graphene sheets. Co-doping of sulfur with nitrogen resulted in more defective sites and further interrupted the graphitic carbon configuration as well as electronic structure of graphene sheets.

Figure 2a displays the elemental composition from XPS analysis. Oxygen content was reduced from 31 at% of GO to 11.11 at% of rGO because of the decomposition of oxygen functional groups. A nitrogen doping level at

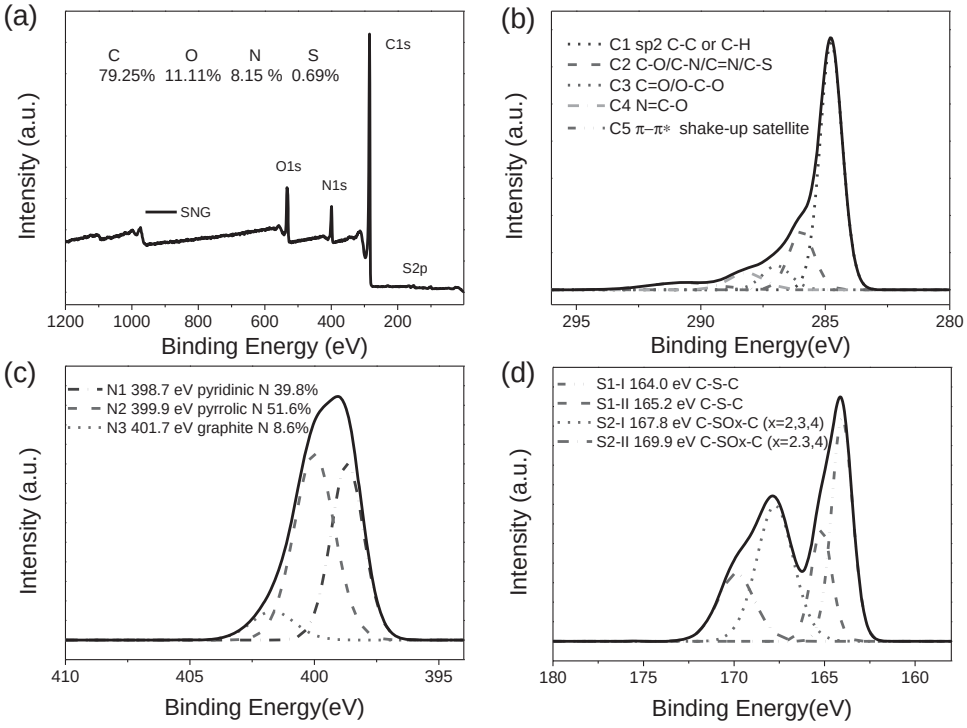

Figure 2. a) XPS survey of SNG, and high resolution XPS b) C1s, c) N1s, and d) S2p.

8.15 at% was achieved, which was higher than that of 3–5 at% via annealing in NH_3 atmosphere and 5.8 at% by a plasma-assisted method.[34,35] Besides, a sulfur doping level of 0.69 at% was obtained. The relatively low S content was attributed to the larger atom radius (1.03 Å vs 0.71 Å of N and 0.75 Å of C), which makes it more difficult to be incorporated into the graphene layer.

The strong peak at the binding energy of 284.8 eV was corresponding to the sp^2-hybridized carbon atoms in the honeycomb lattice. Figure 2b reveals that the C1s can be fitted into five components. The main peak at 284.8 eV was assigned to the sp^2 carbon, suggesting that most of the carbon atoms still remained in the conjugated graphene system,[36] which was further confirmed by the broad peak of shake-up satellite at the binding energy of 290.7 eV. The peak at 285.9 eV (C2) was assigned to the sp^2-carbon bonded with heteroatoms such as C–O, C–N, C=N, and C–S, while the peak at binding energy of 287.0 eV (C3) could be attributed to carbon atoms double-bonded with oxygen atoms such as C=O and/or O–C–O. The peak with a higher binding energy of 288.2 eV was possibly from the carbon atoms that bonded with N and O at the same time (N=C–O).[37]

High resolution XPS N1s was obtained to investigate the doped N species (Figure 2c). It is noted that three types of nitrogen: pyridine-like, pyrrole-like, and quaternary N (also known as graphitic N), were found in SNG with a level of 39.8, 51.6, and 8.6 at% in overall N dopants, respectively. It is well known that a higher temperature could afford more instinct doping of N into the graphene basal plane, whereas elevated temperatures could also break up the C–N bond and result in the loss of nitrogen.[34,38] Besides, the oxygen groups on GO, also as shown in Figure S5, Supporting Information, perform as active sites and bonding reconstruction are necessary for N atoms to be incorporated into the highly conjugated graphene lattice.[31,32,34] Figure S6, Supporting Information, shows the thermal analysis of the samples, indicating that the temperature of removal and decomposition of oxygen-functional groups was at the range of nitrogen doping process.

Chemical states of sulfur dopants were illustrated in Figure 2d. Usually the S p2 peak would split into two linked peaks S p1/2 and S p3/2. The two adjacent peaks at 164.0 and 165.2 eV were assigned to the C–S–C, whereas the peaks at the bind energy of around 167.8 and 169.9 eV were attributable to C–SO_x–C (x = 2, 3, 4).[14,39] The XPS indicated that sulfur atoms were successfully doped into the graphene layer. It is worthwhile noting that the S-doping was achieved in this study by a facile method without any critical synthesis conditions widely used in the previous studies such as CVD or thermal annealing at high temperature.[26,40]

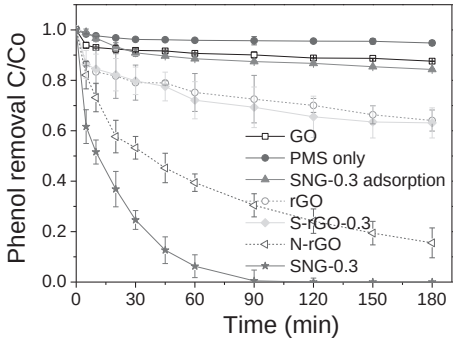

Figure 3. Phenol removal efficiencies on various carbon catalysts.

2.2. Phenol Oxidative Degradation on Nanocarbons

The adsorption and catalytic oxidation profiles of phenol on various nanocarbons are shown in **Figure 3**. It is noted that PMS could rarely oxidize phenol and only 12% of phenol was removed in 180 min. About 15% of phenol removal was achieved by the adsorption of SNG-0.3. The SNG was able to completely degrade phenol in 90 min and demonstrated the best performance for phenol removal. The SNG was more efficient than the rGO prepared by a hydrothermal method and multiwalled carbon nanotubes with 71% and 76% phenol removal, respectively, within 180 min in previous studies.[17,41] The A first-order kinetic model was applied for the evaluation of catalytic phenol oxidation on graphene samples (Equation (1)).

$$\ln\left(\frac{C}{C_0}\right) = -k_{obs} \cdot t \quad (1)$$

SNG-0.3 was found to have an apparent reaction rate constant of 0.043 ± 0.002 min^{-1}, which was 86.6, 22.8, 19.7, and 4.5 folds higher than that of GO, rGO, S-rGO-0.3, and N-rGO, respectively. The reaction rate of SNG for phenol degradation was estimated to be 0.860 ± 0.040 ppm min^{-1}, which was much higher than Co-SBA-15/PMS (0.175 ppm min^{-1}) and Co-ZSM-5/PMS (0.019 ppm min^{-1}) systems.[42,43] In a pioneering study, a N-doped rGO was demonstrated to effectively activate PMS for phenol oxidation with superior degradation efficiency comparable to the most popular metal oxides, such as α-MnO_2 and Co_3O_4.[9] It can be seen that co-doping with nitrogen and sulfur into the graphene layer would further enhance the catalytic performance in phenol oxidation.

Figure 4a presents the effect of the catalyst loading on PMS activation. It is well known that an increase of catalyst dosage can bring out more active sites to react with PMS, hereby dramatically promote the generation of active radicals. More specifically, 75% of phenol was decomposed in 180 min at 0.1 g L^{-1} catalysts, while 100% phenol removal was obtained in 90 and 20 min when the catalyst amount was increased to 0.2 and 0.4 g L^{-1}, respectively.

Phenol removal efficiency was also influenced by the dosage of PMS as shown in Figure 4b. The total duration for 100% phenol degradation was reduced from 150 to 30 min with the addition of PMS from 3.3×10^{-3} M to 26×10^{-3} M. It was found that in the Co_3O_4/PMS system, further increase of PMS loading (more than 6.5×10^{-3} M) would decrease the phenol removal efficiency, owing to the extra SO_5^- in solution reacting with $SO_4^{\bullet-}$ to generate $SO_5^{\bullet-}$, which possesses a lower oxidative potential (1.1 V) than the $SO_4^{\bullet-}$ (2.5–3.1 V).[43,44] However, compared with the metal-based catalyst, SNG presented a greater potential for catalytically activating a high dosage of PMS for phenol decomposition.

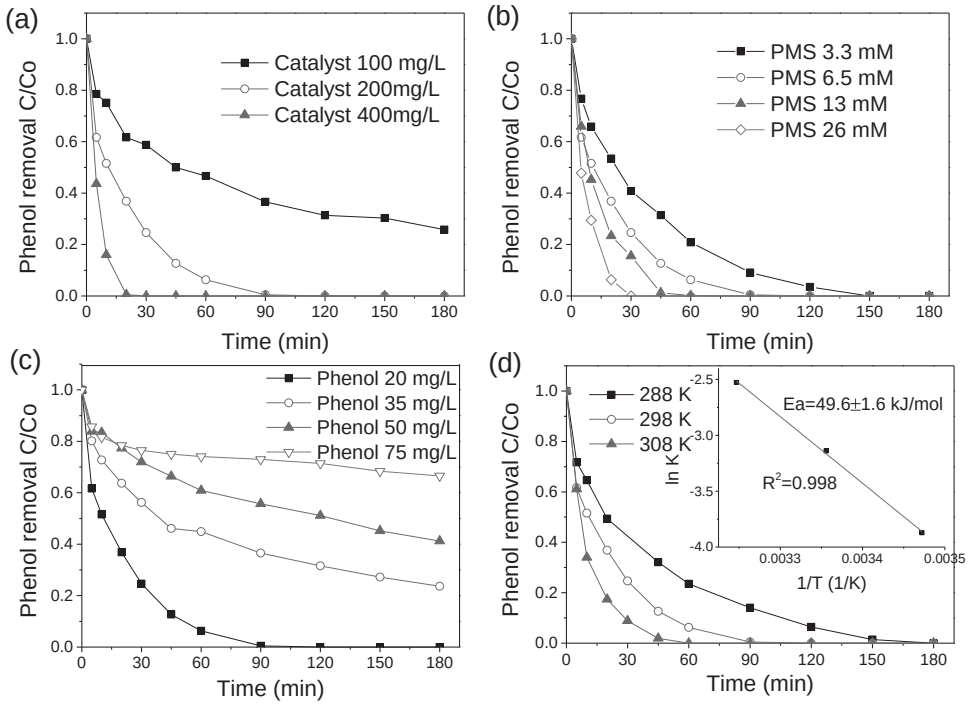

Figure 4. Effects of a) catalyst loading, b) PMS dosage, c) initial phenol concentration, and d) reaction temperature on phenol oxidation on S–N–G.

The influence of initial phenol concentration from 20 to 75 mg L^{-1} was presented in Figure 4c. As expected, the phenol degradation efficiency dropped with the increasing phenol concentration. The apparent reaction rate constants decreased from 0.043 ± 0.002 min^{-1} (R^2 = 0.993) to (9.1 ± 0.8) × 10^{-3} min^{-1} (R^2 = 0.930), (6.2 ± 0.4) × 10^{-3} min^{-1} (R^2 = 0.941) and (3.1 ± 0.5) × 10^{-3} min^{-1} (R^2 = 0.905) with the addition of phenol from 20 to 35, 50, 75 mg L^{-1}, accordingly. It is deduced that the excess adsorption of phenol could cover the active sites of the catalysts, giving rise to the low catalytic activity for PMS activation. Moreover, the low reaction efficiency of phenol oxidation was also possibly due to the deficiency of PMS as the produced active radicals would be quickly consumed by the excess radical inhibitor (phenol and intermediates), thereby slowing down its own consumption by radicals.

Reaction temperature also acts as a significant factor in phenol removal. Figure 4d indicates that a higher reaction rate was achieved at an elevated temperature. For instance, complete phenol degradation was obtained in 60 min at the reaction temperature of 35 °C (k_{obs} = 0.080 ± 0.005 min^{-1}, R^2 = 0.977), compared with 90 min and 180 min of phenol removal at 25 °C (k_{obs} = 0.043 ± 0.002 min^{-1}, R^2 = 0.993) and 15 °C (k_{obs} = 0.021 ± 0.005, R^2 = 0.987), respectively. Based on the Arrhenius equation, the activation energy (E_a) of SNG for catalyzed phenol oxidative degradation was estimated to be 49.6 ± 1.6 kJ mol^{-1}, which was lower than that of pristine graphene (68.4 ± 3.6 kJ mol^{-1}), S-rGO (86.2 ± 2.5 kJ mol^{-1}) in Figure S7, Supporting Information, and typical cobalt based catalysts (59.7–69.7 kJ mol^{-1}),[17,42,45] yet similar to that of N-rGO (48.8 ± 1.9 kJ mol^{-1}). The effect of sulfur level on phenol oxidation is shown in Figure S8, Supporting Information, indicating that sulfur dopant also affected the catalytic activity of rGO.

2.3. Catalytic Mechanism of PMS Activation on Graphene

It was reported that the more electronegative N atoms (3.04 vs 2.55 of carbon) can effectively facilitate electron transfer from the neighboring C and lead to a high charge density of carbon atoms. On the other hand, sulfur has a close electronegativity (2.58) to carbon and can reduce the energy difference of graphene between the highest unoccupied molecular orbital (HOMO) and the lowest unoccupied molecular orbital (LUMO) after doping and alter the electron configuration of sp^2 carbon system.[46–48] Yang and co-workers suggested that the spin density played the dominant role for promoting ORR performance of the S-doped graphene.[14] Zhang et al.[49] reported that S-doped graphene clusters (sulfur or sulfur oxide) distributed at the zigzag edges would induce a larger spin and charge density to neighboring carbon and create more active sites for the ORR reaction. Long et al.[32] suggested quaternary N to be the active sites for selective oxidation of benzylic alcohol. Recent studies also demonstrated that S–N co-doping presented a synergistic effect owing to the redistribution of spin and charge densities and newly created more active sites.[37,40,48]

Density functional theory (DFT) calculations were carried out to give further insights into the effects of dopants on the electron states of carbon atoms in a graphene sheet model (**Scheme 1**). Figures S9–S13, Supporting Information, show the molecular structures and spin densities of pure and modified graphene materials. As seen in **Table 1**, negligible charge transfer among the involving carbon atoms was found in the S-doped graphene, while N doping induces a high positive charge density to the adjacent carbons (C1, C2, and C3). Co-doping of S into the N-doped graphene further increases the charge density of the C2 from 0.31 to 0.48.

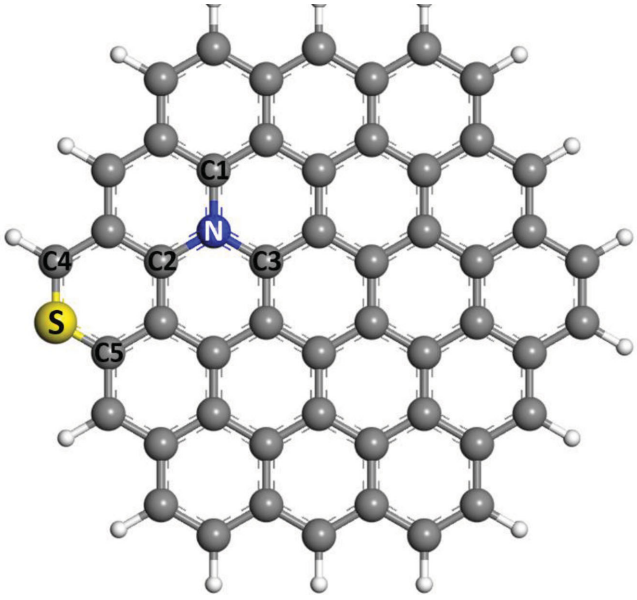

Scheme 1. Molecular model of S-, N-dual doped graphene.

The electrostatic potential mapping in **Figure 5** revealed that the doping process would significantly break the chemical inertness of pristine graphene and change the electron distribution and surface chemistry. The theoretical calculations were consistent with the experimental findings that single sulfur doping presented poor activity for PMS activation (Figure S14, Supporting Information), while N-rGO demonstrated a better performance for phenol removal. Sulfur and nitrogen co-doping demonstrated a greater catalytic activity than pristine graphene and S- or N-doped rGO. We supposed that positively charged carbon sites might be the active sites to facilitate the adsorption of HSO_5^- and break up O–O bond (HO–SO_4^-) in PMS activation.[50] The synergistic effect of S and N co-doping can effectively break the inertness of carbon systems, activate the sp^2-hybridized carbon lattice and facilitate the electron transfer from covalent graphene sheets to PMS for radical generation.

The effect of co-doped sulfur amount was investigated and the enhancement of catalysis was shown in **Figure 6**. The activity increased with the addition of DDS (diphenyl disulfide)from the level of 0.05–0.3 g/g GO and dropped when the DDS/GO was increased to 0.5 g/g, yet still higher than the N-rGO. It was suggested that increasing sulfur amount in a certain range can improve the catalytic performance of phenol oxidative decomposition, yet the synergistic effect would be weakened when superabundant sulfur atoms were introduced into the graphene framework. The excess sulfur might break the charge balance of the covalent graphene electron system and disrupt the charge redistribution when S became the dominant dopant as sole S-doping, presenting a poor catalytic activity as evidenced in Figure S8, Supporting Information. This is further verified by theoretical calculations that the charge density of C1, C2, C3 decreased from 0.26, 0.36, and 0.56 (S–N–G) to 0.08, 0.17, and 0.49 (S–S–N–G), respectively, and that the positive charged area reduced significantly when one more sulfur atom was introduced into the S–N–graphene model (S–S–N–G, Figure 5e). It can be suggested that, compared with metal-based catalysts, the overall catalytic performance for PMS activation on graphene is not simply relying on the increasing of N and S active sites but the contributions from intricately synergistic coupling interactions between the dopants. The same phenomenon was also reported in B and N dual-doped systems.[16]

Table 1. Charge density of atoms in graphene model.

Atom number	Graphene	S-doped graphene	N-doped graphene	S-, N-doped graphene	S-, S-, N-graphene
N	...	...	–0.65	–0.65	–0.68
S	...	0.12	...	1.23	0.58
C1	0.16	0.11	0.29	0.26	0.08
C2	–0.09	0.08	0.29	0.36	0.17
C3	–0.07	0.02	0.58	0.56	0.49
C4	–0.01	–0.38	–0.10	–0.42	0.00
C5	0.05	0.12	0.22	0.06	–0.31

To experimentally probe the PMS activation processes, electron paramagnetic resonance (EPR) was employed to identify the reactive radicals using 5,5-dimethyl-1-pyrroline N-oxide (DMPO) as a spin trapping agent. **Figure 7**a shows that SNG demonstrated an excellent performance for activating PMS to generate active radicals. Radical revolution in Figure 7b reveals that both $SO_4^{\bullet-}$ and $^{\bullet}OH$ were quickly produced in the first five minutes. Their intensities then gradually went down owing to the consumption by phenol oxidation. Huang and co-workers[51,52] applied Fe_3O_4 nanoparticles to activate PMS and found that only $^{\bullet}OH$ was initially generated in the first few minutes and the concentration of $SO_4^{\bullet-}$ climbed up afterwards. The same phenomena also occurred in a CoPc/PMS system. It can be suggested that the radical generation process on nanocarbons might be different from that on metal-based catalysts. Chemically modified graphene can activate PMS to produce both sulfate and hydroxyl radicals effectively for pollutants degradation. It is noted that the relative intensity of DMOP–OH is much higher than that of DPMO–SO_4, suggesting that •OH might play a critical role in phenol degradation, especially in the first few minutes. The competitive radical quenching tests (Figures S14–S16, Supporting Information) indicate that sulfate radicals also presented a great effect in the whole process of phenol oxidation.

Figure S17, Supporting Information, shows the stability of SNG in repeated uses. It should be noted that the stability of the SNG was not comparable to conventional metal-based catalysts. The poor reusability of nanocarbons applied under high oxidant concentration was also found in rGO, N-rGO, and BNG (boron, nitrgoen co-doped graphene) in our previous studies.[9,17] Figures S18 and Table S1, Supporting Information, indicate the possible deactivation mechanism with changed surface chemistry and pore structures, which was due to the strong oxidation process and coverage of adsorbed phenol and intermediates (shown in Figure S19, Supporting Information) which tend to block the pores and interact with sp^2-hybridized carbon lattice. Future studies need be done to design efficient and robust carbocatalysts to improve the

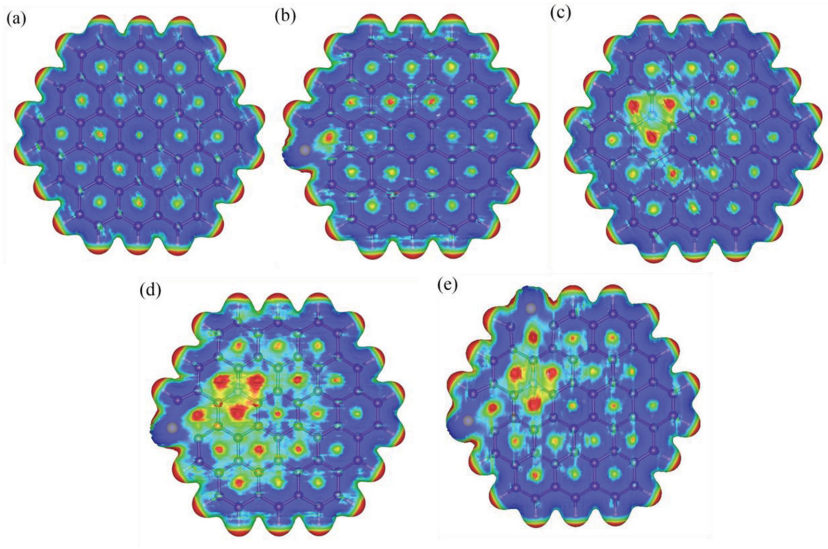

Figure 5. Electrostatic potential mapping from charge density matrix for a) undoped model graphene, b) S–G, c) N–G, d) S–N–G, and e) S–S–N–G.

stability for practical application. Based on above studies, the degradation mechanism was proposed in Scheme S1, Supporting Information. This will provide informative results for future studies on the reusability enhancement.

3. Conclusion

We developed a facile one-pot strategy to successfully incorporate sulfur and nitrogen atoms into graphene sheets. Both experimental and theoretical studies demonstrated that co-dopants (S and N) presented synergistically catalytic activity to enhance the PMS activation compared to the pristine and N- (or S-) sole-doped graphene. Kinetic studies indicated that catalyst loading, PMS dosage, initial phenol concentration, and reaction temperature would pose significant influences on the phenol removal efficiencies. EPR spectra and competitive radical tests suggested that both hydroxyl and sulfate radicals were generated and played critical roles in phenol oxidative decomposition. The theoretical calculations also suggested that introducing sulfur into N-doped graphene can significantly change the surface charge distribution and electrostatic potential of graphene. Experimental results demonstrated that, compared with boron, phosphorus, and iodine, sulfur can function as an effective co-dopant to further enhance catalytic activity of N-doped graphene for phenol degradation with radicals. This study suggested that chemically modified graphene is able to be utilized as a superior metal-free catalyst for sustainable environmental remediation.

4. Computational Methodology

A $C_{54}H_{18}$ cluster was used as a model graphene sheet for DFT calculations. Sulfur was doped at the edge to give two single bonds to adjacent carbons as demonstrated experimentally using XPS.[48] For simplification, only graphitic N doping was considered. For co-doping, the relative positions of S and N were based on a previously reported model for investigation of ORR with various distances from S to N.[48] Electronic structure calculations were carried out using the FHI-aims (Fritz Haber Institute ab initio molecular simulations) all-electron DFT code[53,54] using numerical atom-centered orbitals as a basis set. The default "tight" orbital set was used.

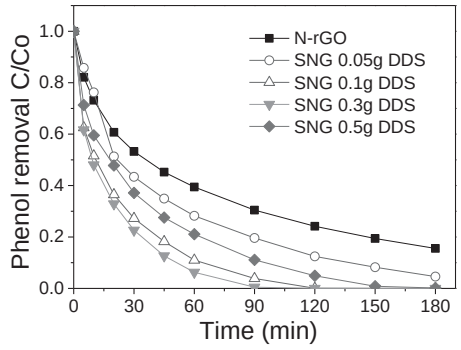

Figure 6. Phenol removal on N-rGO and S, N co-doped rGO with different contents of sulfur precursor (per gram GO) (catalyst: 0.2 g L^{-1}; PMS: 6.5×10^{-3} M; phenol: 20 mg L^{-1}; T: 25 °C).

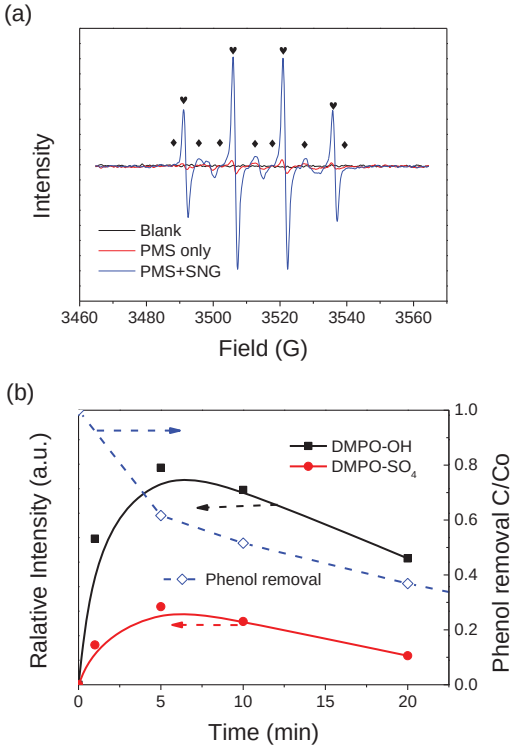

Figure 7. a) EPR spectra of PMS activation under different conditions (♥: DMPO-OH, ♦: DMPO-SO_4). b) Radicals revolution during the PMS activation on SNG (catalyst: 0.2 g L^{-1}; PMS: 6.5×10^{-3} M; phenol: 20 mg L^{-1}; T: 25 °C; DMPO: 0.08 M).

Calculations were performed at the gamma point using the PBE (Perdew-Burke-Ernzerhof) exchange-correlation functional[55] to a SCF (Self-Consistent Field) convergence tolerance of 1×10^{-6} eV. Structures were fully relaxed to a force tolerance of 5×10^{-3} eV Å^{-1}. On-site charges were computed using the Bader analysis via the Bader code.[56] Spin isosurfaces ($n_{up} - n_{down}$) were shown with an isosurface value of 0.007 electrons Å^{-3}. Electrostatic potential were shown with an isosurface value of 0.105 electrons Å^{-3}.

5. Experimental Section

Catalyst Preparation: All the chemicals were purchased from Sigma-Aldrich and used as received without further purification. Graphene oxide (GO) was prepared by a modified Hummers' method.[53] Graphite was oxidized by concentrated H_2SO_4 and $KMnO_4$, and then the produced slurry was reacted with H_2O_2. Details can be found in our previous reports.[9,17] For modified graphene synthesis, finely grounded GO (1.0 g) was dissolved in 100 mL ethanol, stirred for 30 min, and sonicated for 30 min to form a well-dispersed solution. Ammonium nitrate (1.0 g) and diphenyl disulfide (DDS 0.3 g, unless noted elsewhere) were added to the mixture and stirred to dry at 323 K. The product was grounded to fine particles and transferred to a muffle furnace for annealing at 623 K for one hour. The obtained black powder was washed with ultrapure water and ethanol for several times and dried in an oven overnight. Thus S and N co-doped graphene (SNG) sample was obtained. Single nitrogen or sulfur doped graphene (N-rGO or S-rGO-0.3) was prepared by the same procedure above without addition of DDS (or ammonium nitrate). Reduced graphene oxide (rGO) was prepared without addition of any dopant precursors.

Materials Characterization: The morphological information of pristine and modified graphene was investigated by a ZEISS NEON 40EsB scanning electron microscopy (SEM) and a JEOL-2011 transmission electron microscopy (TEM). Raman spectra were acquired on an ISA (Dilor) dispersive. X-ray photoelectron spectroscopy (XPS) was performed on a Kratos AXIS Ultra DLD system with monochromated Al-Kα X-rays (1486.7 eV) under UHV conditions ($<1 \times 10^{-9}$ mbar). Spectra were fitted with Kratos Vision software and CasaXPS software and calibrated to yield a primary C 1s component at 284.5 eV. A Shirley background was applied, fitting with Voigt functions (30% Lorentzian component). Raman spectrometer with argon laser (514 nm). N_2 sorption isotherms were obtained by a Micromeritics Tristar 3000 instrument to determine surface area and pore size distribution. Before analysis, the samples were degassed in vacuum at 100 °C overnight. Electron paramagnetic resonance (EPR) was employed on a Bruker EMS-plus instrument to probe the free radicals. The radicals were trapped with 5,5-dimethyl-1-pyrroline N-oxide (DMPO) and the quantitative information was analyzed by Xeon software (Bruker) with hyperfine splitting constants DMPO-OH: α_N = 14.9 G, α_H = 14.9 G; DMPO-SO_4: α_N = 13.2 G, α_H = 9.6 G, α_H = 1.48G, α_H = 0.78 G.

Catalytic Oxidation Procedure: Phenol oxidation was carried out in a 500 mL conical flask with 20 mg L^{-1} phenol solution and dipped in a constant-temperature water bath (25 °C). The catalyst (0.2 g L^{-1}) was first added to the solution and stirred for 5 min and then PMS (6.5×10^{-3} M) was added to the solution to start the reaction. At each time interval, 1 mL of solution was withdrawn by a syringe, filtered by a 0.45 μm Millipore film, and injected into a HPLC (high performance liquid chromatography) vial. The sample was mixed immediately with 0.5 mL of methanol to quench the reactive radicals, and then analyzed on a Varian HPLC using a UV detector (λ = 270 nm) and a C18 column. The statistical analyses were obtained via performing three parallel experiments on the different carbocatalysts.

Supporting Information

Supporting Information is available from the Wiley Online Library or from the author.

Acknowledgements

This work was financially supported by Australian Research Council (DP130101319). The authors acknowledge the use of equipment, scientific, and technical assistance of the Curtin University Electron Microscope Facility which has been partially funded by the University, State, and Commonwealth Governments, and the WA X-Ray Surface Analysis Facility, funded by the Australian Research Council LIEF grant (LE120100026). H.S. thanks the support from Curtin Research Fellowship.

[1] T. Q. Lin, F. Q. Huang, J. Liang, Y. X. Wang, *Energy Environ. Sci.* **2011**, *4*, 862.
[2] N. Li, Z. P. Chen, W. C. Ren, F. Li, H. M. Cheng, *Proc. Natl. Acad. Sci. USA* **2012**, *109*, 17360.
[3] M. F. El-Kady, V. Strong, S. Dubin, R. B. Kaner, *Science* **2012**, *335*, 1326.
[4] K. N. Wood, R. O'Hayre, S. Pylypenko, *Energy Environ. Sci.* **2014**, *7*, 1212.
[5] H. B. Wang, T. Maiyalagan, X. Wang, *ACS Catal.* **2012**, *2*, 781.
[6] S. Y. Wang, L. P. Zhang, Z. H. Xia, A. Roy, D. W. Chang, J. B. Baek, L. M. Dai, *Angew. Chem. Int. Ed.* **2012**, *51*, 4209.
[7] D. S. Su, J. Zhang, B. Frank, A. Thomas, X. C. Wang, J. Paraknowitsch, R. Schlogl, *Chemsuschem* **2010**, *3*, 169.
[8] D. R. Dreyer, H. P. Jia, C. W. Bielawski, *Angew. Chem. Int. Ed.* **2010**, *49*, 6813.
[9] H. Q. Sun, Y. X. Wang, S. Z. Liu, L. Ge, L. Wang, Z. H. Zhu, S. B. Wang, *Chem. Commun.* **2013**, *49*, 9914.
[10] Y. W. Zhu, S. Murali, W. W. Cai, X. S. Li, J. W. Suk, J. R. Potts, R. S. Ruoff, *Adv. Mater.* **2010**, *22*, 3906.
[11] C. C. Huang, C. Li, G. Q. Shi, *Energy Environ. Sci.* **2012**, *5*, 8848.
[12] X. K. Kong, C. L. Chen, Q. W. Chen, *Chem. Soc. Rev.* **2014**, *43*, 2841.
[13] B. Frank, J. Zhang, R. Blume, R. Schlogl, D. S. Su, *Angew. Chem. Int. Ed.* **2009**, *48*, 6913.
[14] Z. Yang, Z. Yao, G. F. Li, G. Y. Fang, H. G. Nie, Z. Liu, X. M. Zhou, X. Chen, S. M. Huang, *ACS Nano* **2012**, *6*, 205.
[15] Y. Zhao, L. J. Yang, S. Chen, X. Z. Wang, Y. W. Ma, Q. Wu, Y. F. Jiang, W. J. Qian, Z. Hu, *J. Am. Chem. Soc.* **2013**, *135*, 1201.
[16] Y. Zheng, Y. Jiao, L. Ge, M. Jaroniec, S. Z. Qiao, *Angew. Chem. Int. Ed.* **2013**, *52*, 3110.
[17] H. Q. Sun, S. Z. Liu, G. L. Zhou, H. M. Ang, M. O. Tade, S. B. Wang, *ACS Appl. Mater. Interfaces* **2012**, *4*, 5466.

[18] D. E. Jiang, B. G. Sumpter, S. Dai, *J. Chem. Phys.* **2007**, DOI: 10.1063/1.2715558.
[19] S. Z. Liu, W. C. Peng, H. Q. Sun, S. B. Wang, *Nanoscale* **2014**, *6*, 766.
[20] W. C. Peng, S. Z. Liu, H. Q. Sun, Y. J. Yao, L. J. Zhi, S. B. Wang, *J. Mater. Chem. A* **2013**, *1*, 5854.
[21] D. H. Deng, X. L. Pan, L. A. Yu, Y. Cui, Y. P. Jiang, J. Qi, W. X. Li, Q. A. Fu, X. C. Ma, Q. K. Xue, G. Q. Sun, X. H. Bao, *Chem. Mater.* **2011**, *23*, 1188.
[22] C. H. Choi, S. H. Park, S. I. Woo, *ACS Nano* **2012**, *6*, 7084.
[23] C. H. Choi, M. W. Chung, Y. J. Jun, S. I. Woo, *RSC Adv.* **2013**, *3*, 12417.
[24] J. P. Paraknowitsch, A. Thomas, *Energ. Environ. Sci.* **2013**, *6*, 2839.
[25] Y. Z. Su, Y. Zhang, X. D. Zhuang, S. Li, D. Q. Wu, F. Zhang, X. L. Feng, *Carbon* **2013**, *62*, 296.
[26] S. B. Yang, L. J. Zhi, K. Tang, X. L. Feng, J. Maier, K. Mullen, *Adv. Funct. Mater.* **2012**, *22*, 3634.
[27] T. F. Yeh, J. M. Syu, C. Cheng, T. H. Chang, H. S. Teng, *Adv. Funct. Mater.* **2010**, *20*, 2255.
[28] Y. Li, Y. Zhao, H. H. Cheng, Y. Hu, G. Q. Shi, L. M. Dai, L. T. Qu, *J. Am. Chem. Soc.* **2012**, *134*, 15.
[29] L. T. Qu, Y. Liu, J. B. Baek, L. M. Dai, *ACS Nano* **2010**, *4*, 1321.
[30] D. S. Geng, Y. Chen, Y. G. Chen, Y. L. Li, R. Y. Li, X. L. Sun, S. Y. Ye, S. Knights, *Energy Environ. Sci.* **2011**, *4*, 760.
[31] Z. H. Sheng, L. Shao, J. J. Chen, W. J. Bao, F. B. Wang, X. H. Xia, *ACS Nano* **2011**, *5*, 4350.
[32] J. L. Long, X. Q. Xie, J. Xu, Q. Gu, L. M. Chen, X. X. Wang, *ACS Catal.* **2012**, *2*, 622.
[33] Z. R. Ismagilov, A. E. Shalagina, O. Y. Podyacheva, A. V. Ischenko, L. S. Kibis, A. I. Boronin, Y. A. Chesalov, D. I. Kochubey, A. I. Romanenko, O. B. Anikeeva, T. I. Buryakov, E. N. Tkachev, *Carbon* **2009**, *47*, 1922.
[34] X. L. Li, H. L. Wang, J. T. Robinson, H. Sanchez, G. Diankov, H. J. Dai, *J. Am. Chem. Soc.* **2009**, *131*, 15939.
[35] N. A. Kumar, H. Nolan, N. McEvoy, E. Rezvani, R. L. Doyle, M. E. G. Lyons, G. S. Duesberg, *J. Mater. Chem. A* **2013**, *1*, 4431.
[36] J. E. Park, Y. J. Jang, Y. J. Kim, M. S. Song, S. Yoon, D. H. Kim, S. J. Kim, *Phys. Chem. Chem. Phys.* **2014**, *16*, 103.
[37] S. A. Wohlgemuth, R. J. White, M. G. Willinger, M. M. Titirici, M. Antonietti, *Green Chem.* **2012**, *14*, 1515.
[38] K. Kinoshita, Carbon: Electrochemical and Physicochemical Properties, Wiley, New York **1988**.
[39] Y. Yan, Y. X. Yin, S. Xin, Y. G. Guo, L. J. Wan, *Chem. Commun.* **2012**, *48*, 10663.
[40] J. X. Xu, G. F. Dong, C. H. Jin, M. H. Huang, L. H. Guan, *Chemsuschem* **2013**, *6*, 493.
[41] H. Q. Sun, C. Kwan, A. Suvorova, H. M. Ang, M. O. Tade, S. B. Wang, *Appl. Catal. B* **2014**, *154*, 134.
[42] P. Shukla, S. B. Wang, K. Singh, H. M. Ang, M. O. Tade, *Appl. Catal. B* **2010**, *99*, 163.
[43] P. Shukla, H. Q. Sun, S. B. Wang, H. M. Ang, M. O. Tade, *Catal. Today* **2011**, *175*, 380.
[44] E. Saputra, S. Muhammad, H. Q. Sun, H. M. Ang, M. O. Tade, S. B. Wang, *Appl. Catal. B* **2013**, *142*, 729.
[45] P. R. Shukla, S. B. Wang, H. Q. Sun, H. M. Ang, M. Tade, *Appl. Catal. B* **2010**, *100*, 529.
[46] S. Glenis, A. J. Nelson, M. M. Labes, *J. Appl. Phys.* **1999**, *86*, 4464.
[47] N. Kurita, K. Kobayashi, H. Kumahora, K. Tago, K. Ozawa, *Chem. Phys. Lett.* **1992**, *198*, 95.
[48] J. Liang, Y. Jiao, M. Jaroniec, S. Z. Qiao, *Angew. Chem., Int. Ed.* **2012**, *51*, 11496.
[49] L. P. Zhang, J. B. Niu, M. T. Li, Z. H. Xia, *J. Phys. Chem. C* **2014**, *118*, 3545.
[50] X. Duan, H. Sun, Y. Wang, J. Kang, S. Wang, *ACS Catal.* **2014**, *5*, 553.
[51] C. Tan, N. Gao, Y. Deng, J. Deng, S. Zhou, J. Li, X. Xin, *J. Hazard. Mater.* **2014**, *276*, 452.
[52] Z. F. Huang, H. W. Bao, Y. Y. Yao, W. Y. Lu, W. X. Chen, *Appl. Catal. B* **2014**, *154*, 36.
[53] W. S. Hummers Jr., R. E. Offeman, *J. Am. Chem. Soc.* **1958**, *80*, 1339.
[54] V. Blum, R. Gehrke, F. Hanke, P. Havu, V. Havu, X. G. Ren, K. Reuter, M. Scheffler, *Comput. Phys. Commun.* **2009**, *180*, 2175.
[55] J. P. Perdew, K. Burke, M. Ernzerhof, *Phys. Rev. Lett.* **1996**, *77*, 3865.
[56] W. Tang, E. Sanville, G. Henkelman, *J Phys. Condens. Mat.* **2009**, DOI:10.1088/0953-8984/21/8/084204.

Received: December 16, 2014
Revised: January 28, 2015
Published online: March 18, 2015